Numerical analysis of the stability of the Electrohydrodynamic (EHD) electroconvection between two plates

P A Vázquez[1,2], G E Georghiou[3] and A Castellanos[1]

[1]Dpto. de Electrónica y Electromagnetismo, Facultad de Física, Avda. Reina Mercedes s/n, 41012 Sevilla, Spain

[2]Dpto. de Física Aplicada III, E.S.I. Camino de los Descubrimientos s/n, 41092 Sevilla, Spain

[3] Department of Electrical and Computer Engineering, University of Cyprus, 1678 Nicosia, Cyprus

E-mail: pvazquez@us.es

Abstract. The time evolution of the problem of Electrohydrodynamic (EHD) convection in a liquid between two plates is analysed numerically. The equations are nondimensionalized using the ion drift velocity and the viscous time scales. Following the non-dimensionalisation of the respective model, two different techniques have been used to describe the charge evolution, namely the Finite-Element Flux-Corrected Transport Method and the Particle-In-Cell technique. The results obtained with the two schemes, apart from showing good agreement, have revealed the appearance of a two-roll structure not described in previous works. This is investigated in detail for both strong and weak injection.

Keywords: EHD, Finite Elements, PIC, FCT

PACS numbers: 47.65.-d,02.70.Dh,47.11.Fg,52.65.Rr

Submitted to: *J. Phys. D: Appl. Phys.*

1. Introduction

Electrohydrodynamics (EHD) is an interdisciplinary area dealing with the interaction of fluids and electric fields or charges [1]. It lies in the heart of several important industrial processes[2]. Emerging technologies such as microelectromechanical systems (MEMS), bio MEMS and nanotechnology are also related to EHD [3, 4].

In this paper the problem of the two-dimensional electroconvective flow between two plates immersed in a dielectric liquid is studied. When the applied voltage is high enough the electric force produces an instability that put the liquid into motion. This is a classical Electrohydrodynamic (EHD) problem that has been considered by several authors. A review of the linear and non linear stability regimes can be found in [5]. Experimental studies have also been conducted [6, 7, 8], however only for strong injection regimes. In particular, Chicón *et al* [9] carried out numerical simulations, imposing a roll structure to the velocity, finding the linear and non-linear stability criterion numerically. They also studied the oscillations of the current and the amplitude of the velocity roll. In a previous paper [10] the authors have used this problem to compare the performance of two different numerical techniques, namely the Flux-Corrected Transport (FCT) [11, 12] and the Particle-in-Cell [13, 14], in dealing with the distribution of electric charge. The imposed velocity roll structure described in [9] was used to simplify the problem and make direct comparisons between the two schemes. It was found that both techniques were capable of describing adequately the steep gradients of the electric charge, with some minor differences in the evolution of the amplitude of the velocity roll.

In this work the full model is considered by incorporating the computation of the velocity field rather than imposing one. The electric charge at the injector electrode is given an initial value and the simulation is carried out until the flow pattern stabilises. As it was the case in [10], two different sets of numerical techniques have been used, namely (1) Finite Elements combined with the Particle-in-Cell method (FE-PIC) and (2) Finite Elements and the Flux-Corrected Transport Method (FE-FCT). Both weak and strong injection have been studied with respect to stability and structure of the flow. The FE-PIC method has been used for the strong injection case while the FE-FCT was used in the weak one. The reason is the different simulation times required in the two cases. The weak injection case requires more time to develop the velocity roll, and the FE-FCT is significantly faster than the FE-PIC. However some of the simulations have been carried out with both schemes, in order to be sure that both methods give the same results.

As it was mentioned above, the analytical stability studies, both linear and non-linear, impose a one-roll structure and look both for the threshold value of the stability parameter and the most unstable wavelength. The same technique is used in the numerical work in [9] and [10]. From our simulations, it turns out that the flow pattern is more complex than this single roll structure. In the strong injection limit, for a high enough value of the stability parameter, the one roll structure evolves into a two-roll pattern, for a cell length half the wavelength of the value obtained from the stability

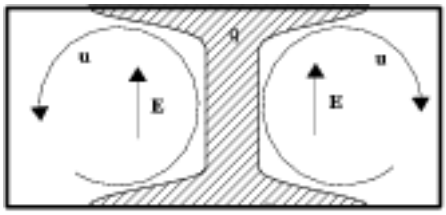

Figure 1. Typical flow pattern and distribution of electric charge for the electroconvection between two plates.

analysis. In the weak injection limit the flows adopts a two-roll structure for all values of the stability parameter.

The paper is arranged as follows. Firstly, an analysis of the time scales of the problem is considered in order to choose the best time scales to describe the time evolution. It can be shown that the optimum is the viscous time. Four non-dimensional parameters can be typically considered: the electric Reynolds number Re_E, the stability parameter T, the injection strength parameter C and the mobility parameter M, but only three of them are needed in order to fully define the problem. We retain the parameters C, T and M, the latter one not because of its physical meaning, but due to the fact that it provides a good way of identifying the liquid. However, as we are interested in studying the stability of the flow, we fix the values of Re_E and T. M is then computed from these two parameters. From an experimental point of view this implies changing the liquid. Subsequently, results of simulations obtained by neglecting the convective term are presented, in order to investigate its significance on the evolution of the flow pattern. As the value of the velocity obtained in the simulations implies that the convective term is not negligible, another set of simulations has been run this time solving the full EHD problem including the convective term too. Once more the two-roll structure has been found to develop. Finally, in order to eliminate the effect of the boundaries on the charge evolution, simulations in a much wider domain have been considered and the flow pattern was found to be much more complex than what could be expected from the linear stability analysis. The results suggest that the complexity is mainly attributed to the coupling between the electric charge and the velocity.

2. Problem formulation

Two plane electrodes of length L_x and a distance d apart immersed in a non-conductive fluid are considered. The system is considered to extend infinitely along the transversal direction so that the flow can be taken as two-dimensional. An electric potential is applied between the plates so that injection of charge occurs. The electric field forces the charges away from the injector and in this way a space charge appears. The Coulomb force pushes the charges and the liquid with them. If the electric potential is high enough all the liquid is put into motion with the roll structure shown in figure 1. The linear stability for this type of problem has been studied by several authors. A review of

the linear and non linear stability studies can be found in [5]. The problem has also been studied numerically by Chicón *et al* [9], where they imposed a velocity roll before finding the linear stability criterion and studying the oscillations of the current and the amplitude of the velocity roll. In that study it was confirmed that the stability criteria did not depend on the value of the mobility parameter M.

The fluid is considered to be incompressible, isothermal and insulating with mass density ρ, kinematic viscosity ν and permittivity ε. An electric voltage Φ_0 is applied between the plates. When the electric field is high enough, electric charge is injected from the electrodes into the liquid. Unipolar injection is assumed where only one of the electrodes injects. The charge carriers are considered to be of the same type with an ionic mobility K so they migrate along the liquid with a velocity $K\mathbf{E}$, where $\mathbf{E}$ is the electric field. The injection is further assumed to be autonomous so the density of charge at the injector is constant and equal to q_0, and that the ions discharge instantaneously once they reach the opposite electrode.

There are three mechanisms responsible for the motion of ions: convection by the fluid, drift by the electric field and molecular diffusion. The last one can be neglected [1] so the current density is given by $\mathbf{J} = q(K\mathbf{E} + \mathbf{u})$, $\mathbf{u}$ being the velocity of the fluid. The first term represents drift and the second one convection. Complete characterisation of the problem can be given by the following dimensional equations incorporating Poisson's equation for the field and Navier-Stokes equations for the fluid:

$$\nabla^2\Phi = -q/\varepsilon, \qquad \mathbf{E} = -\nabla\Phi \tag{1}$$

$$\nabla \cdot \mathbf{J} + \frac{\partial q}{\partial t} = 0, \tag{2}$$

$$\nabla \cdot \mathbf{u} = 0, \tag{3}$$

$$\frac{\partial \mathbf{u}}{\partial t} + \mathbf{u} \cdot \nabla\mathbf{u} = -\frac{1}{\rho}\nabla p + \nu\nabla^2\mathbf{u} + \frac{1}{\rho}q\mathbf{E}, \tag{4}$$

where Φ is the electric potential, q the charge density and p the pressure. The domain geometry and the boundary conditions are shown in figure 2.

We are interested in studying the time evolution of the system, in order to describe the evolution of the fluid pattern and the distribution of electric charge. As we will see later, we have chosen as scale for the velocity the ionic drift velocity, that is, $U_0 = KE_0 = K\Phi_0/d$. This is the natural selection when studying the onset of convection, because the roll structure starts developing when the velocity of the fluid is of the same order than the drift velocity of the ions [1, 5, 9]. As the scale for the spatial dimension is d, the natural time scale is $t_0 = d/U_0 = d^2/K\Phi_0$ that happens to be the drift time τ_d. However, the different phenomena encountered in this kind of problems involve a host of time scales. The time step of our simulations must be small enough to catch all the different mechanisms involved in the system. This is the reason why we have compared the different time scales in order to take the smaller one for the non-dimensionalization of the problem. In the next section we analyze these time scales.

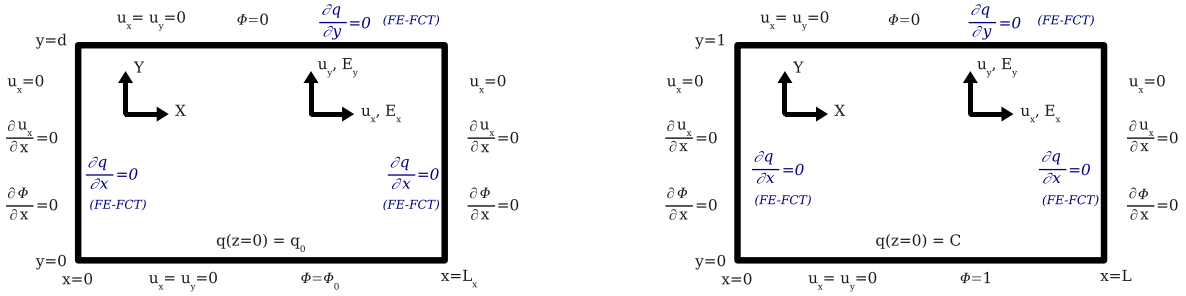

Figure 2. Dimensional (left) and non-dimensional (right) computational domain and boundary conditions for the problem. The additional charge boundary conditions for FE-FCT along the symmetry and top boundaries are written in blue color and italic face.

2.1. Analysis of time scales

The relevant time scales of the problem are the viscous time, τ_ν, the drift time, τ_d, and the Coulomb repulsion time, τ_C,

$$\tau_\nu = d^2/\nu, \qquad \tau_d = d^2/K\Phi_0, \qquad \tau_C = \varepsilon/Kq_0. \tag{5}$$

The viscous time τ_ν comes from the balance between the temporal derivative and the viscous term in (4) and represents the time that diffusion requires to propagate a perturbation in the velocity in the domain. The drift time τ_d is the time that an ion needs to travel the distance between the plates moving with the drift velocity $K\mathbf{E}$. The repulsion time τ_C is the time needed by Coulomb repulsion to dissipate a density of charge. It arises from equation (2) when diffusion of electric charge is neglected [1], yielding:

$$\frac{\partial q}{\partial t} + (\mathbf{u} + q\mathbf{E}) \cdot \nabla q = \frac{\mathrm{d}q}{\mathrm{d}t} = -\frac{q^2 K}{\varepsilon}. \tag{6}$$

Hence, τ_ν is related to the velocity distribution and τ_d and τ_C are related to the charge distribution. It is interesting to compare these times

$$\begin{aligned} \tau_C/\tau_d &= \varepsilon\Phi_0/q_0 d^2 = 1/C, \\ \tau_d/\tau_\nu &= \nu/K\Phi_0 = 1/Re_E, \\ \tau_C/\tau_\nu &= \varepsilon\nu/Kq_0 d^2 = 1/Re_E\, C. \end{aligned} \tag{7}$$

Here C is the injection strength parameter and Re_E is the electric Reynolds number, built with the ion velocity. They are defined as

$$C = \frac{q_0 d^2}{\varepsilon\Phi_0}, \qquad Re_E = \frac{K\Phi_0}{\nu} \tag{8}$$

In experiments, C can take a large range of values. When $C \ll 1$ the regime is said to be of weak injection. In this case the electric space charge does not affect significantly the electric field distribution. When $C \gg 1$ the regime is of strong injection, and the electric field is controlled by the space charge. For Re_E, the experimental values are $Re_E \sim 10^{-2} - 1$ [1, 6, 7, 8, 18]. For the work presented in this paper $C = 0.1$ and $C = 10$ are considered as typical values for weak and strong injection, respectively. Now, it is instructive to look for the smallest of the typical times present.

Weak injection $C = 0.1$: In this case $\tau_\nu \lesssim \tau_d \ll \tau_C$. So the smallest time is τ_ν.

Strong injection $C = 10$: In this case it is $\tau_C \ll \tau_d,\ \tau_C \sim \tau_\nu,\ \tau_\nu \lesssim \tau_d$. This merits more careful consideration. From the experimental values of Re_E two limit cases must be considered: $Re_E \simeq 10^{-2}$ and $Re_E \simeq 1$. For the former case $\tau_C \simeq 10\tau_\nu$, so τ_ν is still the dominant time. However, for the latter case $\tau_C \simeq 0.1\tau_\nu$, so the charge evolves quicker than the velocity field.

To conclude, in all the cases the smallest time step is the viscous time, τ_ν, except when $C = 10$ and $Re_E = 1$. Therefore we have chosen τ_ν as the time scale for the nondimensonalization. As it is discussed below, in the numerical scheme, we choose a time step $\Delta t = 10^{-3} \simeq 10^{-2}\tau_C$. So, even in the special case in which the repulsion time is smaller than the viscous one, the numerical simulation is able to describe accurately and efficiently the evolution of the system.

There are two other non-dimensional parameters that can be defined

$$T = \frac{\varepsilon \Phi_0}{\rho \nu K}, \qquad M = \frac{1}{K}\left(\frac{\varepsilon}{\rho}\right)^{1/2} \tag{9}$$

The stability parameter T is defined as the ratio between the force and viscous terms in the Navier-Stokes equation. The mobility parameter M [19] is obtained from the balance between the densities of electric and hydrodynamic energy, $\varepsilon E^2/2 \sim \rho U^2/2$. In this way a hydrodynamic mobility can be defined $K_H = (\varepsilon/\rho)^{1/2}$, where ε and ρ are the permittivity and the mass density of the fluid so that, in the turbulent regime, we have $U = K_H E$, E and U being the typical values of the electric and velocity fields. Then $M = K_H/K$, where K is the ion mobility.

Only three non-dimensional parameters are needed. Usually the parameters T, C and M are chosen. The parameter M is retained because it characterises the properties of the liquid. So the electric Reynolds number is written as $Re_E = T/M^2$. We can now arrive to the non-dimensional equations.

2.1.1. Non-dimensional problem The scales for all the involved variables are

$$\begin{array}{lll} x, y \simeq d & \Phi \simeq \Phi_0 & E \simeq \Phi_0/d \\ u \simeq K\Phi_0/d & t \simeq \tau_\nu = d^2/\nu & p \simeq \rho K \Phi_0 \nu/d \\ q \simeq \varepsilon \Phi_0/d^2 & & \end{array} \tag{10}$$

From these non-dimensional electric and hydrodynamic equations become:

$$\nabla^2 \Phi = -q, \qquad \mathbf{E} = -\nabla \Phi, \tag{11}$$

$$\frac{T}{M^2}\nabla \cdot [q(\mathbf{u} + \mathbf{E})] + \frac{\partial q}{\partial t} = 0, \tag{12}$$

$$\nabla \cdot \mathbf{u} = 0, \tag{13}$$

$$\frac{\partial \mathbf{u}}{\partial t} + \frac{T}{M^2}(\mathbf{u} \cdot \nabla)\mathbf{u} = -\nabla p + \nabla^2 \mathbf{u} + Tq\mathbf{E}, \tag{14}$$

The non-dimensional domain and boundary conditions are shown in figure 2.

The selection for the scale of the pressure is somewhat awkward. Usually it is the electric pressure, $\varepsilon {E_0}^2$ or the dynamic pressure, $\rho {U_0}^2$ which are used. However, in this problem the absolute value of the pressure is not relevant. With the chosen scale there are no parameters in front of the pressure gradient and this produces a symmetric matrix in the numerical scheme.

3. Numerical algorithms

In this section the two numerical schemes used in the work are briefly described. Then results of simulations in the Stokes regime, where the convective term in (14) is neglected, are presented. As it turns out that the magnitude of the fluid velocity is not consistent with neglecting convection in the momentum equation, a set of simulations with the full Navier-Stokes equations has been carried out. The results from this computations are discussed.

3.1. Numerical procedure

Two different numerical techniques have been used to solve the problem. On one hand the combined Finite Element and Particle in Cell (FE-PIC) method and, on the other hand, the Finite Element-Flux Corrected Transport (FE-FCT) method. In each case we solve the problem defined by equations (11) to (14) in the domain defined by figure 2 with the boundary conditions also depicted in figure 2. The length L of the domain depends on the value of the injection parameter. We use the value of half the wavelength given by the linear stability analysis [15], that is, $L = 0.687$ for $C = 0.1$ and $L = 0.614$ for $C = 10$.

We have used the FE-PIC method for the strong injection regime and the FE-FCT method for the weak injection case. The two algorithms have been compared and validated for similar problems in previous work [10]. The reason for this decision is that in the weak injection case the development of the flow is much slower, and the FE-FCT is considerably faster than FE-PIC. In any case, the most important results have been verified with both techniques.

In particular, for the FE-FCT (weak injection, C=0.1), an unstructured triangular mesh of 3000 nodes with minimum element quality of 0.54 has been used, with high resolution at the top and bottom electrodes expanding outwards from the left boundary. For FE-PIC (strong injection, C=10) a structured quadrangular mesh of 1581 velocity nodes and 416 pressure and electrical nodes has been used, with higher resolution near the boundaries. More details of the numerical schemes are given below.

3.1.1. Finite Element - Particle-in-Cell (FE-PIC) Method Given a distribution of electric charge density in the domain, this is simulated with an initial set of particles whose charge is assigned to the mesh. The charge of each particle is divided amongst the elements where the charge is present [13, 14]. Then Poisson's equation is solved on

the mesh using finite elements and the electric field is computed along with the charge density. Using this the velocity field is computed from the Navier-Stokes equations. Once the fluid velocity and electric field are known at each node their values are interpolated at the position of each particle. These are then displaced by a certain distance. The solution progresses iteratively. The Navier-Stokes equations are solved with a fractional-step finite element method [16]. An intermediate velocity is computed, taking into account the boundary conditions. Then the pressure is calculated using the usual Pressure Schur Complement approach. In this step a lumped mass matrix is used. At the last step, the velocity is computed, including also the boundary conditions. The algorithm has been implemented using Taylor-Hood elements, with quadratic elements for velocity and linear for pressure. The electric potential is computed on the same mesh, using linear elements. The charge density is taken as uniform in each element. The electric field at each node is computed as the average of its values in the elements where the node is present.

In order to study the stability of the hydrostatic solution, the computation is first done in the absence of a velocity field, that is, the particles are driven only by the electric field, until a steady state is reached. This state corresponds to the hydrostatic solution. The computation proceeds from this point.

Summarizing, the main steps in the particle-mesh calculation are:

(i) put particles in the domain.
(ii) assign the charge of the particles to the mesh.
(iii) solve Poisson's equation for the electric potential and calculate the electric field.
(iv) calculate the velocity field using finite-elements.
(v) interpolate the electric field and the fluid velocity at the super-particle positions.
(vi) move the super-particles.
(vii) go back to step 1 until a steady state is reached.

3.1.2. Finite Element Flux-Corrected-Transport (FE-FCT) Method The numerical algorithm used for the solution of the continuity equation for charges and the Navier-Stokes equations is based on the improved FE-FCT method developed by the authors and is described in its three-dimensional form in [17]. The FCT method essentially uses a low order (that includes diffusion) and a higher order scheme (that is oscillatory) to reconstruct the optimal solution. The flux limiting procedure which is at the heart of the FCT combines the two schemes (low and high order) in a nonlinear way to produce the optimal solution which is free from excess diffusion and oscillation. The two-step Lax-Wendroff method is used to obtain a high order solution. Then, using mass lumping, the low order scheme is constructed with a variable diffusion coefficient based on the Courant number, as it is considered to be the optimal diffusion coefficient. This diffusion coefficient is not the same as the actual diffusion in the equations. The limiting procedure proposed by Zalesak for multidimensional problems is finally invoked

to provide an accurate and ripple-free solution for the charge densities, and Poisson's equation is solved by the same standard finite element solver as for the PIC case. The use of unstructured grids associated with finite elements reduces significantly the number of unknowns and hence computing time for a given problem through the use of fine resolution only where steep gradients occur. The modelling of complex geometries is then made possible maintaining at the same time the ability to capture those steep gradients (through the FCT part).

The solution procedure assumes an initial distribution of ions along with given values of velocity, density, temperature and pressure at an applied voltage. The two step Lax-Wendroff scheme is employed for this algorithm. More details can be found in [11]. The charged particle densities at time n are fed to Poisson's equation to obtain the electric field distribution at time n (E_n). Then these are passed to the charge particle continuity equation to calculate the charge densities at time n + 1/2. Next, the charge densities, electric field and transport properties at time n are passed to the Navier-Stokes solver to calculate the velocity field at time n + 1/2. Subsequently the charge particle densities are passed to the Poisson solver to calculate the electric field at time n + 1/2. This completes the half time step solution. The most recently found electric and velocity field values are then fed to the charge particle continuity solver to calculate the charge densities at time n + 1. Finally, the transport parameters, the electric field and the charge densities at time n + 1/2 are used by the Navier-Stokes solver to obtain the velocity field at time n + 1. The flow chart in figure 3 describes the whole procedure in a more graphical way.

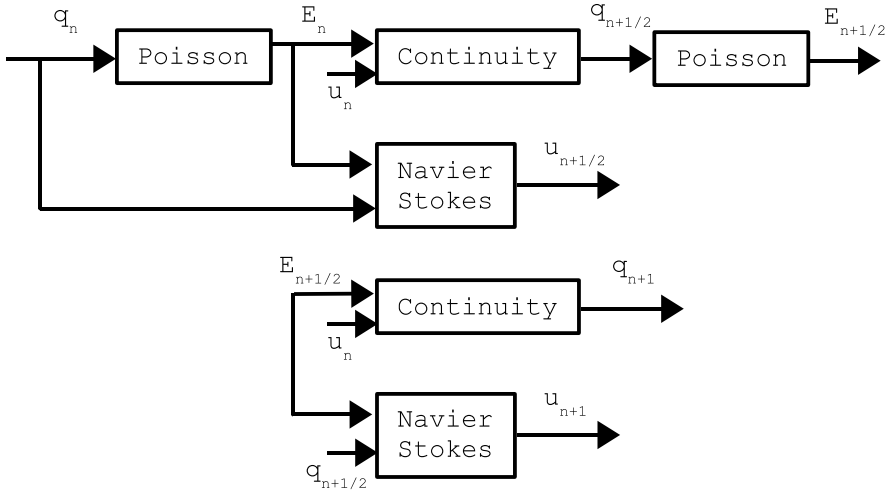

Figure 3. Flow chart for the numerical procedure described in section 3.1.2

As it is pointed out in the introduction, the FE-PIC technique has been used for strong injection and the FE-FCT technique for weak injection, as the latter one takes less computation time. As an example, a typical simulation with FE-PIC takes about 10 hours, while a typical simulation with FE-FCT takes about 3 hours, both for a 2

GHz processor.

3.2. Results

In this section results for the electroconvective flux between two plates are presented. The simulations in the Stokes regime where the convective term in (14) is neglected, are considered first. Then the convective terms are also included in the model and simulations are presented in both the weak and strong injection cases. The results section is completed with simulations in a wider domain so that the effects of the boundaries on the occurrence of the two roll structure can be identified. Some very interesting results have been obtained with regards to the appearance of a two roll structure not previously observed and an attempt is made to analyse the mechanism behind its appearance.

3.2.1. Simulations in Stokes regime The first part of the work involved the investigation of the stability and further evolution of the system for the Stokes regime, that is, taking a small value of $Re_E = T/M^2$ so the convective terms can be neglected in (14). The FE-PIC method has been used once more for the strong injection case, whereas the FE-FCT was employed for the weak injection case. Only the strong injection case is discussed here.

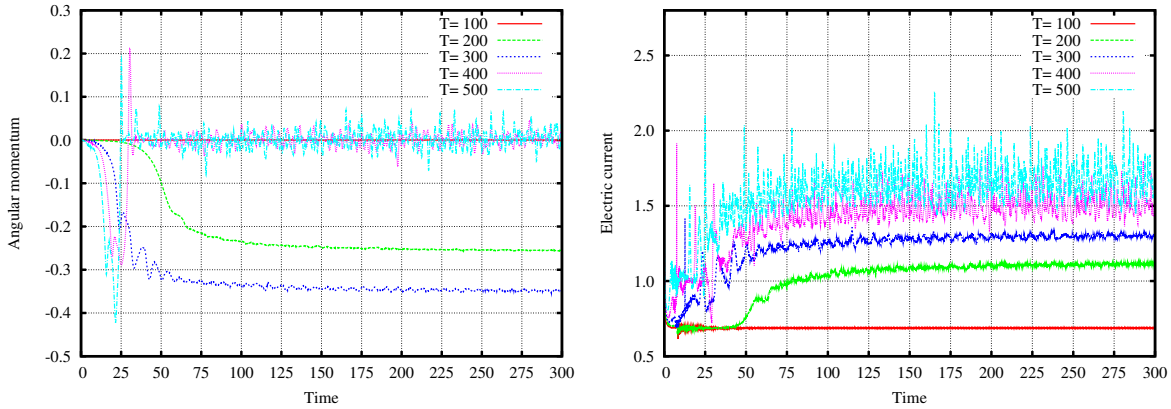

Figure 4. Evolution of the angular momentum (left) and the electric current (right) for Stokes regime with $C = 10$, $Re_E = 0.1$ and $T = 100 - 500$. These simulations have been carried out with the FE-PIC method. The electric current is computed along the line $y = 0.5$. Note that there are no units associated with the parameters, as the non-dimensional equations have been used.

The simulations were carried out for $Re_E = 0.10$ and $T = 100 - 1000$. Figure 4 shows the time evolution of the angular momentum of the flow for $T = 100, 200, 300, 400$ and 500. The angular momentum is computed with respect to the center of the domain of calculation, that is $\int_{\text{cell}}(\mathbf{r} - \mathbf{r}_0) \times \mathbf{u}\, \mathrm{d}S$, $\mathbf{r}_0$ being the position vector of the center. For $T = 100$ no roll develops. For $T = 200$ and 300 we get a one-roll structure, and the angular momentum acquires a steady value. The roll develops faster for greater

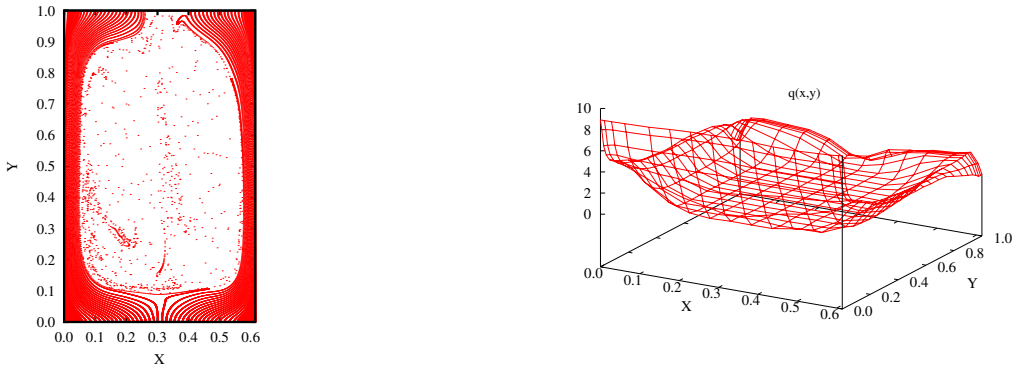

Figure 5. Distribution of particles (left) and charge density (right) for $C = 10$, $Re_E = 0.1$ and $T = 500$ for $t = 100$ for Stokes regime with FE-PIC.

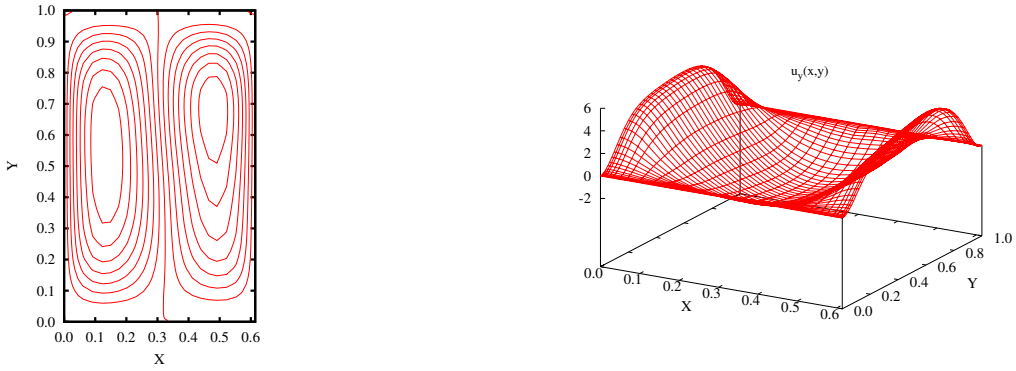

Figure 6. Stream function contour plot (left) and component u_y (right) for $C = 10$, $Re_E = 0.1$ and $T = 500$ for $t = 100$ for Stokes regime with FE-PIC.

T. These results are similar to those obtained in previous works [1, 5, 9]. The linear instability threshold in our simulations is about $T = 163$, very close to the theoretical one, $T = 161$.[15]. A significant change can be observed for $T = 400$ and $T = 500$. A roll develops, as in the previous cases, but at around $t = 40$ the value of the angular momentum falls to zero and begins to oscillate around this value. These cases ($T = 400, 500$) correspond to a two roll structure, with the velocity field and the electric charge density distribution oscillating. The behaviour is similar for the rest of the values of T up to 1000. The two-roll structure produces large oscillations in the electric current around the steady state value. Figure 4 shows the evolution of the current intensity per unit length for the same values of T. With one roll ($T = 200$ and 300) the current increases with respect to the stationary case ($T = 100$) reflecting the augmentation of the total velocity of the charges due to convection. The current attains a steady value, with small oscillations. These oscillations increase when the two-roll structure appears for $T >= 400$. Figure 5 shows the distribution of particles and charge density in the domain for a non-dimensional time $t = 100$ and $T = 500$. The two-roll structure is clearly seen. The charges leave the central region and follow the upcoming fluid at both sides of the cell. Figure 6 shows the streamlines and the y component of the velocity

for the same situation.

Results obtained with the FE-FCT method for the weak injection case are similar, except that no one-roll structure develops. When the system is set into motion, a two-roll structure develops for all values of T above the linear instability threshold.

However, a problem arises when looking at the maximum value of the y component of the velocity, u_y, in figure 6. The maximum value of u_y is $U_{nd} \sim 10$. If we consider in this case the relative order of magnitude of the convective and diffusive terms in equation (14), that is, the hydrodynamic Reynolds number, we get

$$Re_H = \frac{Re_E(\mathbf{u}\cdot\nabla)\mathbf{u}}{\nabla^2\mathbf{u}} \sim Re_E\, U_{nd} \sim 0.6. \tag{15}$$

So for these values of the parameters the outcome of the simulation is not consistent with the assumption that the convective term is negligible. The situation is even worse for $Re_E = 1$. Similar results are obtained for the weak injection regime using the FE-FCT. This can indicate that, if this new instability is physical, its origin is not due to the non-linear properties of the flow. Nevertheless, in order to ensure that neglecting convection is not critical, a set of simulations solving the whole hydrodynamic problem has been carried out. The results are presented below.

3.2.2. Simulations with convective terms Results from simulations are presented in this section, where the full problem defined by equations (11) to (14) with boundary conditions given in figure 2 is used. A set of simulations for strong injection, $C = 10$, and weak injection, $C = 0.1$, have been carried out using the FE-PIC and the FE-FCT, respectively.

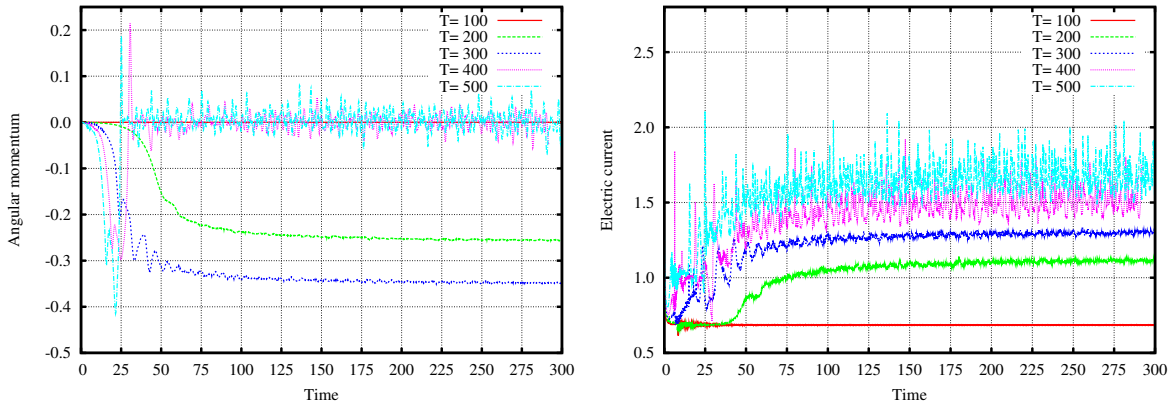

Figure 7. Angular momentum (left) and electric current evolution (right) in time when the convective terms are included. The simulations have been carried out with FE-PIC for $C = 10.0$, $Re_E = 0.1$ and $T = 100 - 500$. The electric current is computed along the line $y = 0.5$.

Strong injection, C=10 (FE-PIC) Figure 7 shows the angular momentum and the electric current for $C = 10$, $Re_E = 0.1$ and $T = 100 - 500$ including the convective

terms. The behaviour is quite similar to the Stokes regime case. Near the instability onset, the velocity is still small, and the convective terms are not so important. When the flow pattern is fully developed, the differences are greater, but the two-roll structures and the oscillations appear again for $T = 400, 500$, as the oscilaltions around zero of the angular momentum for these values show. The distribution of electric charge and velocity are similar to that shown in figures 5 and 6. The fact that the two roll structure appears again could indicate that the complexity of the flow pattern, if real, arises more from the coupling between the electric charge distribution and the velocity field than from non linear components in the flow.

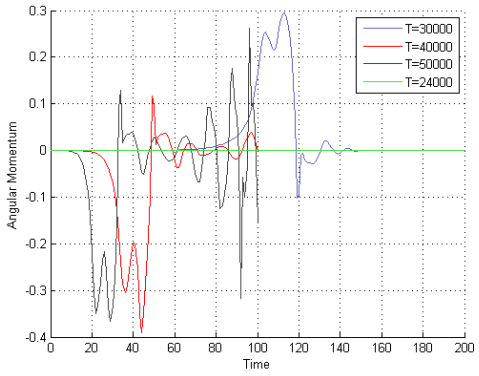

Figure 8. Angular momentum evolution in time for the weak injection case. The simulations have been carried out with the FE-FCT for $C = 0.1$ and $Re_E = 0.1$.

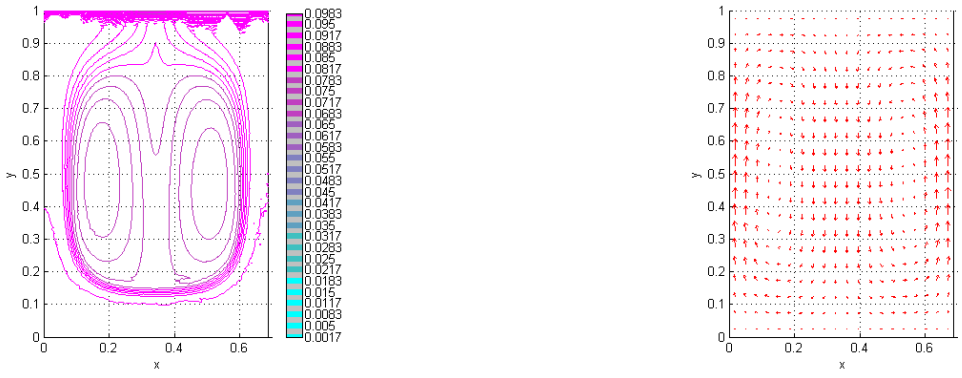

Figure 9. Electric charge density distribution (left) and velocity field (right) in the weak injection regime for $t = 150$. The simulation has been carried out with FE-FCT for $C = 0.1$ and $Re_E = 0.1$ including convective terms for $T = 30\,000$.

Weak injection, C=0.1 (FCT) The simulations for weak injection, that is, a small value of C, have been produced using the FE-FCT technique. Figures 8 and 9 show the outcome from these simulations. Figure 8 clearly demonstrates that in this case a stable one-roll structure is not obtained for any value of T. For $T = 24\,000$ no roll develops,

which is consistent with the theoretical limit and the results from [9]. For $T = 30\,000$ a roll develops at $t \approx 60$, but it becomes a two-roll structure at $t \approx 120$. Higher values of T reproduce this behaviour, the only difference is that the instabilities develop earlier in time. Figure 9 shows the distribution of the charge density and the flow pattern for $T = 30\,000$ and $t = 150$. The two-roll structure is clearly seen, similar to that obtained for the Stokes regime with strong injection. As the non existence of a stable roll is somewhat surprising, a set of simulations with the same parameters has been reproduced using the FE-PIC. Although the results are not shown here, the outcome is similar, both the values of the velocity obtained and the behaviour of the flow agree, confirming the above observations.

3.2.3. Analysis of the two roll structure In this section the development of the two-roll structure is further analysed in order to obtain useful insight regarding its development.

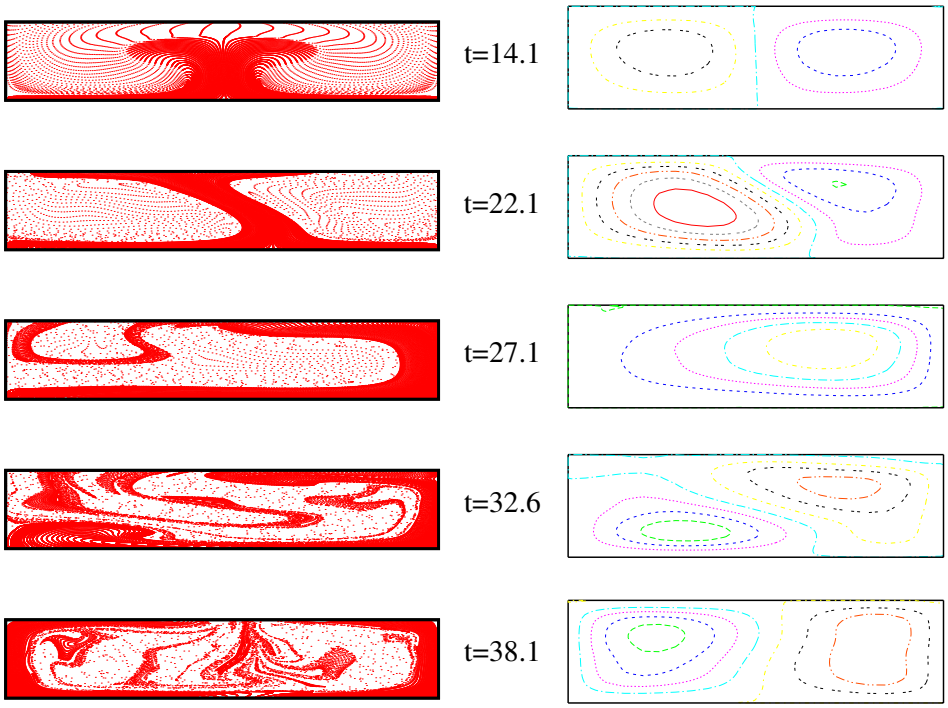

Figure 10. Evolution of the two-roll structure for $C = 10$, $Re_E = 0.1$ and $T = 800$. The plots correspond to times t=14.1, 22.1, 27.1, 32.6, 38.1. The left column shows the particle distribution and the right column the stream function. The proportion between the height and the length are not respected for the sake of clarity.

The results obtained by using the FE-PIC method for $C = 10$, $Re_E = 0.1$ and $T = 800$ at different times are shown in figure 10. The development of the first instability is apparent. In fact the instability develops with a two-roll pattern flow, as the charge accumulates towards the central part of the cell. There, a plume rises entraining the charge from the injector to the opposite electrode. At later times, $t = 22 - 27$ in figure

Figure 11. Particle distribution (left) and stream function (right) for $L = 4 * L_{\text{linear}}$, $C = 10$, $Re_E = 1.0$ and $T = 400$ with FE-PIC. at time $t = 6.0$. Up to seven rolls can be discerned. The boundary conditions are no-slip at the right and left sides.

10, the plume twists to one side and the pattern flow exhibits a one-roll structure. This behaviour is similar for values of T in the range $T = 200 - 300$ as shown in figure 7 where the single roll remains.

However, for greater values of T, the roll becomes unstable. At $t = 32.6$ a smaller velocity roll at the bottom left corner starts developing. This roll pushes electric charge from the bottom, as it is seen in the particle distribution plot for $t = 32.6$. Eventually, this blob of charge arrives to the top electrode, and a two-roll structure is attained. The pattern is more or less stable, although great oscillations of the positions of the centres of the rolls occur, which produce significant fluctuations in the angular momentum and electric current, as can be seen in figure 7.

Now, for the blob of charge appearing at the bottom left corner to get to the opposite electrode, it must overcome the downward velocity component from the main roll. This can happen only if the main roll becomes weaker and its center moves to the right, leaving space for the charge to go up. This corresponds to the great oscillations in angular momentum seen in figure 7 for $T = 400, 500$ just before the mean value drops to zero. Then, it is the instability of the main roll that allows the development of the secondary roll, which, eventually, becomes as important as the main one.

3.2.4. Simulations for wider cells The two-roll structure can be due to a spurious effect introduced by the imposed boundary conditions at the lateral walls of the cell. As a result, simulations with a cell several times wider than the linear value of L have been carried out, imposing no-slip boundary conditions to the velocity. For weak injection $L = 10 * L_{\text{linear}} = 6.87$ has been used with the FE-FCT method , while for strong injection $L = 4 * L_{\text{linear}} = 2.456$ has been imposed in conjunction with the FE-PIC method.

Figure 11 shows the particle distribution and the stream function contour plot for $t = 6.0$, $C = 10$, $Re_E = 1.0$ and $T = 400$. Seven rolls can be seen but the pattern is not stable. The total number of rolls changes from two to even eight. If the roll structure used in linear and non-linear analysis was stable then four rolls would appear in all

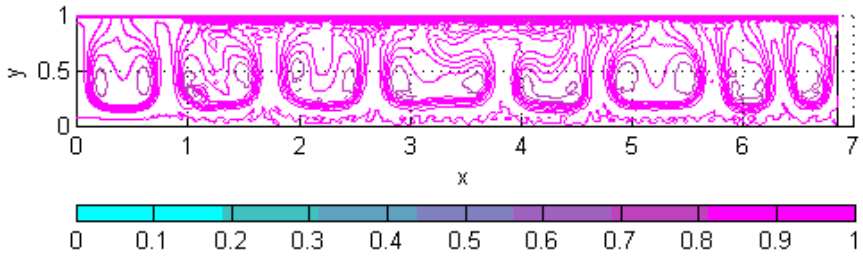

Figure 12. Charge density distribution for $L = 10 * L_{lineal}$, $C = 0.1$, $Re_E = 0.1$ and $T = 30\,000$ with FE-FCT at time $t = 100$. At least 16 rolls are present, more that the 10 rolls used in the linear and non linear analysis. The boundary conditions are no-slip at the right and left sides.

cases. Similar conclusions can be deduced from figure 12, where the result from a FE-FCT simulation for the weak regime has been produced. In this case the width of the cell is $10L_{\text{linear}}$. At least 16 velocity rolls can be seen. It is worth noting that between every column of charge in figure 12 there are two velocity rolls turning in opposite directions.

From the above results it becomes apparent that the complexity inherent in the full problem cannot be described with the roll structure used in the linear and non-linear stability analysis. It is interesting to remark that this complex behaviour appears also in the Stokes regime, showing that the instability is more related to the electric charge distribution than to non-linear effects in the fluid.

Some comments must be made about the feasibility of experiments to validate these results. Because we have chosen to vary independently Re_E and T, the value of M changes and, consequently, the experiments would involve different liquids. The values of M in our simulations vary from 30 to 70 for strong injection and 500 to 700 for weak injection. Silicone fluids, due to their great range of viscosities, can fulfill these requirements. Several experimental studies concerning these liquids can be found in [1].

4. Conclusions

Results from numerical simulations for the electroconvective flow between two plates carried out using two different sets of numerical techniques have been presented, namely Finite Elements combined with Particle-in-Cell method (FE-PIC) and Finite Elements and the Flux-Corrected Transport Method (FE-FCT). The former has been used for the strong injection regime and the latter for the weak injection regime for both Stokes and full convective regimes, although the most relevant results have been verified using both techniques. The viscous time has been used as time scale, as it is the smallest one

in typical experimental condition.

In this work we have found that, at least in our numerical tests and for the case of roll structures, the pattern flow issued from the non-linear stability analysis turns out to be unstable when the liquid motion is fully developed. For values of the stability parameter T consistent with previous analysis the fluid is put into motion. For strong injection (C=10), when T is slightly above the stability threshold, a stable single roll structure appears when the width of the cell is chosen according to the previous stability analysis. However as T increases, a two-roll structure develops. This pattern is more or less stable, although oscillations of the positions of the centres of the rolls and their amplitudes occur. For weak injection the two-roll appears from the very beginning of the instability onset. This fact has been verified with both numerical algorithms and the same behaviour occurs in both the Stokes and convective regimes. This may indicate that the instability does not arise from the non-linear aspects of the flow, but rather from the details of the coupling between the distribution of electric charge and the velocity flow.

Finally, simulations with cells several times wider than the linear width have been carried out. There it can be seen that the flow is very unstable, making it very difficult to define a wavelength. This is a strong indication that the complexity does not arise from the boundary conditions imposed at the lateral walls. Of course it is important to say that these are only numerical results and they should be verified by experiments.

Acknowledgments

This work has been supported by the Spanish Ministerio de Ciencia y Tecnología under contract FIS2006-03645 and the Junta de Andalucia under contract FQM-421.

References

[1] Castellanos A ed 1998 *Electrohydrodynamics* (New York: Springer-Verlag) [2, 4, 5, 11, 16]

[2] Cowley J M 1986 *Fundamentals of Applied Electrostatics* (New York: Wiley) [2]

[3] De Voe D L , Darabi J and Ohadi M 2001 An electrohydrodynamic polarization micropump for electronic cooling applications *J. of Microelectromech. Syst.* **10** 98–106 [2]

[4] Gonzalez A, Green N G, Castellanos A, Ramos A and Morgan H 2003 Electrohydrodynamics and dielectrophoresis in microsystems: scaling laws. *J. Phys. D: Appl. Phys.* **36** 2584–2597 [2]

[5] Atten P 1996 Electrohydrodynamic instability and motion induced by injected space charge in insulating liquids. *IEEE Trans. Dielectr. Electr. Insul.* **3** 1–17 [2, 4, 11]

[6] Schneider J M and Watson P K 1970 Electrohydrodyamic stability of space-charge-limited currents in dielectric liquids ii. experimental study. *Phys. Fluids* **13**(8) 1955 – 1961 [2, 5]

[7] Atten P and Malraison B 1982 Chaotic behavior of instability due to unipolar ion injection in a dielectric liquid. *Phys. Rev. Lett.* **49**(10) [2, 5]

[8] Pontiga F, Castellanos A and Malraison B 1995 Some considerations on the instabilities of nonpolar liquids subjected to charge injection. *Phys. Fluids* **7**(6) 1348 – 1356 [2, 5]

[9] Chicón R, Castellanos A and Martín E 1997 Numerical modelling of coulomb-driven convection in insulating liquids. *J. Fluid Mech.* **344** 43–66 [2, 4, 11, 14]

[10] Vazquez P A, Georghiou G E and Castellanos A 2006 Characterization of injection instabilities in electrohydrodynamics by numerical modelling: comparison of particle in cell and flux corrected

transport methods for electroconvection between two plates. *J. Phys. D: Appl. Phys.* **39** 2754 – 2763 [2, 7]

[11] Georghiou G E, Morrow R and Metaxas A C 1998 An improved finite-element flux corrected transport algorithm *J. Comput. Phys.* **148** 605 – 620 [2, 9]

[12] Georghiou G E, Morrow R and Metaxas A C 2000 A two-dimensional finite element - flux corrected transport algorithm for the solution of gas discharge problems *J. Phys. D: Appl. Phys.* **33** 2453 – 2466 [2]

[13] Hockney R W and Eastwood J W 1981 *Computer Simulations using Particles* (New York: McGraw-Hill) [2, 7]

[14] Bridsall C K and Langdon A B 1991 *Plasma Physics via Computer Simulation* (Bristol: Institute of Physics Publishing) [2, 7]

[15] Atten P and Moreau R 1972 Stabilité électrohydrodynamique des liquides isolants soumis à une injection unipolaire *J. Méc.* **11** 471 – 520 [7, 11]

[16] Blasco J, Codina R and Huerta A 1998 A fractional-step method for the incompressible navier-stokes equations related to a predictor-multicorrector algorithm. *Internat. J. Numer. Methods Fluids* **28** 1391–1419 [8]

[17] Hallac A, Georghiou G E and Metaxas A C 2002 Three dimensional algorithm for transient gas discharge processes–Validation *Int. Conf. on Gas Discharges and Applications (Liverpool, England)* pp 315-18 [8]

[18] Castellanos A 1991 Coulomb-driven convection in electrohydrodynamics *IEEE Trans. Electr. Insul.* **26**(6) 1201 – 1215 [5]

[19] Felici N 1969 Phénomenes hydro et aérodynamiques dans la conduction des diélectriques fluides *Rev. Gen. Electrostat.* **78** 717 – 734 [6]